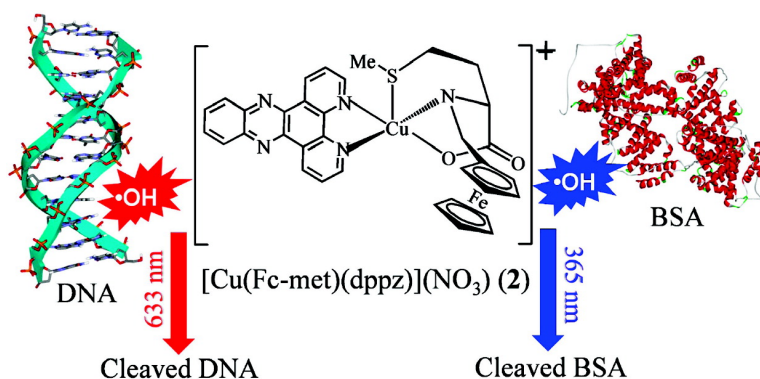


Photoinduced DNA and Protein Cleavage Activity of Ferrocene-Appended L-Methionine Reduced Schiff Base Copper(II) Complexes of Phenanthroline Bases

Tridib K. Goswami, Mithun Roy, Munirathinam Nethaji, and Akhil R. Chakravarty

Organometallics, 2009, 28 (7), 1992-1994 • DOI: 10.1021/om900012b • Publication Date (Web): 03 March 2009

Downloaded from <http://pubs.acs.org> on April 29, 2009



More About This Article

Additional resources and features associated with this article are available within the HTML version:

- Supporting Information
- Access to high resolution figures
- Links to articles and content related to this article
- Copyright permission to reproduce figures and/or text from this article

[View the Full Text HTML](#)



ACS Publications
High quality. High impact.

Photoinduced DNA and Protein Cleavage Activity of Ferrocene-Appended L-Methionine Reduced Schiff Base Copper(II) Complexes of Phenanthroline Bases

Tridib K. Goswami, Mithun Roy, Munirathinam Nethaji, and Akhil R. Chakravarty*

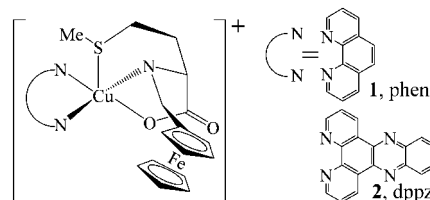
Department of Inorganic and Physical Chemistry, Indian Institute of Science, Bangalore 560012, India

Received January 7, 2009

Summary: Ferrocene-appended ternary copper(II) complexes of phenanthroline bases having CuN_3OS coordination with an axial $\text{Cu}-\text{S}$ bond derived from L-methionine reduced Schiff base shows red light induced oxidative DNA cleavage activity following a hydroxyl radical pathway. The dipyrrophenazine complex, in addition, displays photoinduced oxidative cleavage of bovine serum albumin protein in UV-A light.

Bioorganometallic chemistry is an emerging area in chemical biology for varied use of organometallic complexes in therapeutic applications.^{1–5} Ferrocene, its conjugates, and other metallocenes have been used in chemotherapeutic studies.^{6–10} The impetus derives from the stability of the ferrocene moiety in biological medium. In addition, it is nontoxic, lipophilic, and redox-active. The presence of the ferrocenyl moiety (Fc) enhances the therapeutic activity of ferrocifen, the ferrocene-appended anticancer drug tamoxifen, and ferroquine, the ferrocene-attached antimalarial drug chloroquine ($\text{Fc} = (\eta^5\text{-C}_5\text{H}_4\text{Fe}(\eta^5\text{-C}_5\text{H}_5))$).^{9,10} Bioorganometallic complexes are also useful as sensors for DNA, proteins, environmental pollutants, and food additives.^{11,12} In addition to ferrocene-based compounds, arene–ruthenium complexes are useful as antimetastasis agents to control tumor malignancy.^{1,13,14} The present work stems from our interests in exploring the chemistry of bioor-

Scheme 1. Schematic Representation of the Complexes 1 and 2



ganometallic complexes as synthetic photonucleases by designing ferrocene-conjugated 3d-metal complexes showing DNA cleavage activity within the photodynamic therapy (PDT) spectral window of 600–800 nm.¹⁵ In this communication we report the red light induced DNA cleavage activity of two ferrocene-appended reduced Schiff base (Fc-met) copper(II) complexes of L-methionine and phenanthroline bases, namely, $[\text{Cu}(\text{Fc-met})(\text{B})](\text{NO}_3)_2$, where B is 1,10-phenanthroline (phen) for **1** and dipyrro[3,2-*a*:2',3'-*c*]phenazine (dppz) for **2** (Scheme 1).

The complexes were prepared by reacting the ferrocene-conjugated reduced Schiff base ligand with copper(II) nitrate and the phenanthroline base (B) in methanol and characterized from analytical and physicochemical data (Table S1 and Figures S1–S4 in the Supporting Information).¹⁶ Complex **1**, as its PF_6 salt (**1a**), was structurally characterized by X-ray crystallography (Tables S2 and S3 and Figures S5 and S6 in the Supporting Information).¹⁷ The crystal structure shows a square-pyramidal ($4 + 1$) geometry of $\text{Cu}(\text{II})$ with a CuN_3OS coordination in which the tridentate NOS-donor monoanionic Fc-met ligand shows axial coordination of the sulfur of L-methionine, giving a $\text{Cu}(\text{II})-\text{S}$ bond distance of $\sim 2.68 \text{ \AA}$ (Figure 1). The phen ligand shows N,N coordination. The chiral carbon of L-methionine has the *S*-configuration. The Fc unit shows an eclipsed conformation.

Complexes **1** and **2** showed quasi-reversible cyclic voltammetric responses at -0.06 and -0.03 V for the $\text{Cu}(\text{II})-\text{Cu}(\text{I})$

* To whom correspondence should be addressed. Fax: 91-80-23600683. E-mail: arc@ipc.iisc.ernet.in.

(1) Allardyce, C. S.; Dorcier, A.; Scolaro, C.; Dyson, P. J. *Appl. Organomet. Chem.* **2005**, *19*, 1–10.

(2) Hartinger, C. G.; Dyson, P. J. *Chem. Soc. Rev.* **2009**, *38*, 391–401.

(3) Jaouen, G.; Vessieres, A.; Butler, I. S. *Acc. Chem. Res.* **1993**, *26*, 361–369.

(4) Fish, R. H.; Jaouen, G. *Organometallics* **2003**, *22*, 2166–2177.

(5) Alberto, R. J. *Organomet. Chem.* **2007**, *692*, 1179–1186.

(6) (a) Johnson, T. R.; Mann, B. E.; Clark, J. E.; Foresti, R.; Green, C. J.; Motterlini, R. *Angew. Chem., Int. Ed.* **2003**, *42*, 3722–3727. (b) Erker, G. J. *Organomet. Chem.* **2007**, *692*, 1187–1197.

(7) Fouda, M. F. R.; Abd-Elzaher, M. M.; Abdelsamaia, R. A.; Labib, A. A. *Appl. Organomet. Chem.* **2007**, *21*, 613–625.

(8) Van Staveren, D. R.; Metzler-Nolte, N. *Chem. Rev.* **2004**, *104*, 5931–5985.

(9) Nguyen, A.; Top, S.; Vessieres, A.; Pigeon, P.; Huche, M.; Hillard, E. A.; Jaouen, G. J. *Organomet. Chem.* **2007**, *692*, 1219–1225.

(10) Biot, C.; Glorian, G.; Maciejewski, L. A.; Brocard, J. S.; Domarle, O.; Blampain, G.; Millet, P.; Georges, A. J.; Abessolo, H.; Dive, D.; Lebibi, J. J. *Med. Chem.* **1997**, *40*, 3715–3718.

(11) (a) Schn, P.; Degefa, T. H.; Asaftei, S.; Meyer, W.; Walder, L. J. *Am. Chem. Soc.* **2005**, *127*, 11486–11496. (b) Immoos, C. E.; Lee, S. J.; Grinstaff, M. W. *J. Am. Chem. Soc.* **2004**, *126*, 10814–10815.

(12) (a) Wu, D.; Huang, W.; Lin, Z.; Duan, C.; He, C.; Wu, S.; Wang, D. *Inorg. Chem.* **2008**, *47*, 7190–7201. (b) Wilson, G. S.; Hu, Y. *Chem. Rev.* **2000**, *100*, 2693–2709.

(13) (a) Liu, H.-K.; Berners-Price, S. J.; Wang, F.; Parkinson, J. A.; Xu, J.; Bella, J.; Sadler, P. J. *Angew. Chem., Int. Ed.* **2006**, *45*, 8153–8156. (b) Yan, Y. K.; Melchart, M.; Habtemariam, A.; Sadler, P. J. *Chem. Commun.* **2005**, 4764–4766.

(14) (a) Bergamo, A.; Sava, G. *Dalton Trans.* **2007**, 1267–1272. (b) Dyson, P. J.; Sava, G. *Dalton Trans.* **2006**, 1929–1933.

(15) Maity, B.; Roy, M.; Chakravarty, A. R. *J. Organomet. Chem.* **2008**, *693*, 1395–1399.

(16) The complexes were prepared by a general synthetic method in which Fc-metH (0.35 g, 1.0 mmol) was treated with $\text{LiOH} \cdot \text{H}_2\text{O}$ (0.038 g, 1.0 mmol) followed by addition of $\text{Cu}(\text{NO}_3)_2 \cdot 3\text{H}_2\text{O}$ (0.24 g, 1.0 mmol) in MeOH (10 mL) and the phenanthroline base (B: phen, 0.19 g; dppz, 0.29 g; 1.0 mmol). The dark green solid was isolated on slow evaporation of the solvent, washed with aqueous MeOH, and dried under vacuum over P_4O_{10} (yield: 0.54 g, 83% for **1**; 0.61 g, 81% for **2**). Anal. Calcd for $\text{C}_{28}\text{H}_{28}\text{N}_4\text{O}_5\text{FeCu}$ (**1**): C, 51.58; H, 4.33; N, 8.59. Found: C, 51.39; H, 4.51; N, 8.36. ESI-MS in MeOH: m/z 589 $[\text{M}-(\text{NO}_3^-)]^+$. UV–visible in DMF-Tris-HCl buffer (1/4 v/v; $\lambda_{\text{max}}/\text{nm}$ ($\epsilon/\text{M}^{-1} \text{ cm}^{-1}$): 597 (140), 437 (255), 272 (24 360). $\mu_{\text{eff}} = 1.83 \mu_{\text{B}}$ at 298 K. Anal. Calcd for $\text{C}_{34}\text{H}_{30}\text{N}_6\text{O}_5\text{FeCu}$ (**2**): C, 54.15; H, 4.01; N, 11.14. Found: C, 53.89; H, 4.18; N, 10.88. ESI-MS in MeOH: m/z 691 $[\text{M}-(\text{NO}_3^-)]^+$. UV–visible in DMF-Tris-HCl buffer (1/4 v/v; $\lambda_{\text{max}}/\text{nm}$ ($\epsilon/\text{M}^{-1} \text{ cm}^{-1}$): 594 (135), 436 (325), 376 (6915), 358 (6770), 273 (36 590). $\mu_{\text{eff}} = 1.81 \mu_{\text{B}}$ at 298 K.

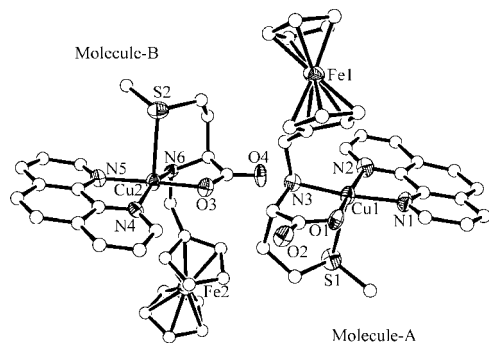


Figure 1. Perspective view of the cationic complex in **1a** showing thermal ellipsoids at the 50% probability level and the atom-numbering scheme for the metal and heteroatoms.

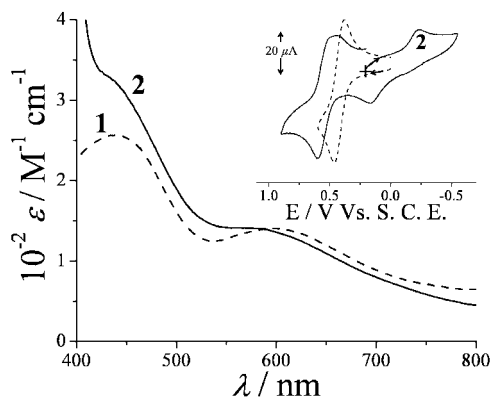


Figure 2. Visible electronic spectra of the complexes **1** and **2** in DMF–Tris–HCl buffer (1/4 v/v). The inset shows the cyclic voltammetric responses of **2** (—) and ferrocene (---) in DMF–0.1 M TBAP at a scan rate of 50 mV s⁻¹.

couple along with the reversible Fc⁺–Fc couple at 0.47 and 0.53 V versus SCE in DMF–0.1 M [Bu₄N](ClO₄), respectively (Figure 2). The one-electron paramagnetic complexes ($\mu_{\text{eff}} \approx 1.8 \mu_{\text{B}}$) showed a weak d–d band near 600 nm and a Fc-centered charge transfer band at ~450 nm in DMF–Tris–HCl buffer (1/4 v/v) (Figure 2). Complex **2**, in addition, displayed a ligand-centered band at ~370 nm involving the phenazine moiety of the dppz ligand.

The binding affinity of the complexes to calf thymus (CT) DNA was studied by spectral and viscosity methods (Figures S7 and S8 in the Supporting Information).¹⁸ Both complexes showed significant DNA binding propensity, giving binding constant values (K_b) of $[7.5(\pm 0.3)] \times 10^4 \text{ M}^{-1}$ for **1** and $[3.7(\pm 0.5)] \times 10^5 \text{ M}^{-1}$ for **2** in Tris–HCl buffer (pH 7.2). Thermal DNA denaturation studies in phosphate buffer (pH 6.85) revealed a stabilizing interaction of the complexes with CT DNA, giving a ΔT_m value of 2.1 °C for **1** and 4.2 °C for **2** (Figure 3). The ΔT_m data indicate primarily the groove-binding

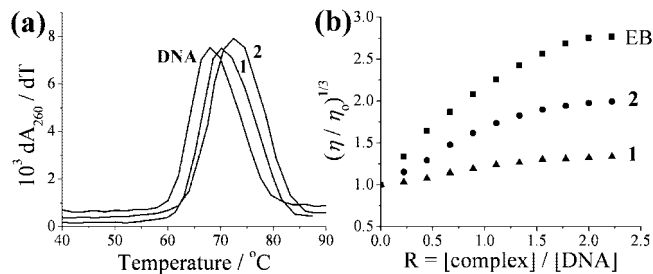


Figure 3. (a) Derivative plots showing DNA melting temperatures using CT DNA (70 μM) in the absence and presence of complexes **1** and **2** (20 μM). (b) Effect of addition of the increasing concentration of ethidium bromide (EB) (■), **1** (▲), and **2** (●) on the relative viscosity of 150 μM CT DNA in 5 mM Tris–HCl buffer (pH 7.2) at 37 °C.

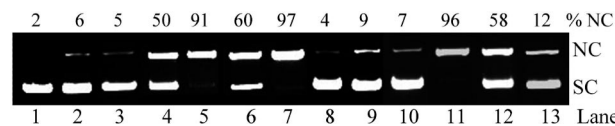


Figure 4. Gel electrophoresis diagram showing the visible light induced SC pUC19 DNA (0.2 μg , 30 μM bp) cleavage activity of the complexes [Cu(Fc-met)B](NO₃) (B = phen for **1** and dppz for **2**) (30 μM) for a photoexposure time of 2 h: lane 1, DNA control (454 nm); lane 2, DNA + **1** (in the dark for 2 h); lane 3, DNA + **2** (in the dark for 2 h); lane 4, DNA + **1** (454 nm); lane 5, DNA + **2** (454 nm); lane 6, DNA + **1** (633 nm); lane 7, DNA + **2** (633 nm); lane 8, DNA + distamycin (633 nm); lane 9, DNA + methyl green (633 nm); lane 10, DNA + distamycin + **1** (633 nm); lane 11, DNA + distamycin + **2** (633 nm); lane 12, DNA + methyl green + **1** (633 nm); lane 13, DNA + methyl green + **2** (633 nm).

nature of the complexes. Viscometric data showed significant change in the relative specific viscosity of the complexes. The effect for the dppz complex **2** was found to be significantly higher than that of the phen complex **1**, suggesting the partial DNA intercalative binding propensity of complex **2** (Figure 3).

We explored the photoinduced DNA cleavage activity of the complexes using supercoiled (SC) pUC19 DNA (0.2 μg , 30 μM bp) in Tris–HCl/NaCl buffer (pH 7.2) using visible laser radiation of wavelengths 633 nm (12 mW, continuous-wave (CW) He–Ne laser) and 454 nm (30 mW, CW Ar–Kr laser).¹⁹ The wavelengths chosen for photoirradiation of the samples corresponded to the absorption bands near 450 and 600 nm. Both complexes showed efficient photoinduced DNA cleavage activity (Figure 4). A 30 μM solution of **1** showed ~60% cleavage of SC DNA to its nicked circular (NC) form on d–d band excitation at 633 nm for 2 h, while **2** cleaved >90% of SC DNA. Photoexcitation of the Fc-centered band near 454 nm led to ~50% and ~90% cleavage of SC DNA by **1** and **2** (30 μM), respectively.

Mechanistic investigations were done using various additives to understand the nature of the reactive species involved in the DNA cleavage reactions (Figure S9 in the Supporting Informa-

(17) Crystal data for [Cu(Fc-met)(phen)](PF₆): C₂₈H₂₈CuF₆FeN₃O₂PS, $M = 734.97$, triclinic, $P1$, $a = 10.790(5) \text{ \AA}$, $b = 11.048(5) \text{ \AA}$, $c = 14.823(5) \text{ \AA}$, $\alpha = 68.657(5)^\circ$, $\beta = 85.234(5)^\circ$, $\gamma = 64.677(5)^\circ$, $V = 1482.1(11) \text{ \AA}^3$, $Z = 2$, $\rho = 1.647 \text{ g cm}^{-3}$, $T = 293(2) \text{ K}$, $1.48 \leq \theta \leq 25^\circ$, $\mu = 14.01 \text{ cm}^{-1}$, $F(000) = 746$, $\text{GOF} = 1.004$, $R1 = 0.0538$, $wR2 = 0.1333$ for 7444 reflections with $I > 2\sigma(I)$ and 775 parameters ($R1(F^2) = 0.0712$ (all data)). $w = [\sigma^2(F_o^2) + (0.0904P)^2 + 0.0000P]^{-1}$, where $P = [F_o^2 + 2F_c^2]/3$ (Bruker SMART APEX CCD diffractometer with Mo K α X-ray source). The structure was solved and refined using the SHELX program: Sheldrick, G. M. SHELX-97, Programs for Crystal Structure Solution and Refinement; University of Göttingen, Göttingen, Germany, 1997.

(18) Roy, M.; Pathak, B.; Patra, A. K.; Jemmis, E. D.; Nethaji, M.; Chakravarty, A. R. *Inorg. Chem.* **2007**, *46*, 11122–11132.

(19) DNA cleavage experiments were carried out using SC pUC19 DNA (0.2 μg , 30 μM bp) in 50 mM Tris–HCl/50 mM NaCl buffer (pH 7.2) containing 5% DMF. The light sources used were a Spectra Physics Water-Cooled Mixed-Gas Ion Laser Stabilite 2018-RM for 454 nm (30 mW, CW beam diameter at $1/e^2$ $1.8 \pm 10\%$ mm, beam divergence $0.7 \pm 10\%$ mrad) and a CW He–Ne Laser of Research Electro-Optics made for 633 nm (12 mW, beam diameter of 0.88 mm, beam divergence of 0.92 mrad). The complex and reagent concentrations corresponded to those in the 20 μL sample volume (solution path length 5 mm). The percentage of DNA cleavage was measured from the band intensities in agarose gels using the UVITECH Gel Documentation System.

tion). The complexes were cleavage inactive under an argon atmosphere. There was no apparent inhibition in the DNA cleavage activity of the complexes in the presence of singlet oxygen ($^1\text{O}_2$) quenchers such as NaN_3 (500 μM), 2,2,6,6-tetramethyl-4-piperidone (TEMP, 500 μM), and L-histidine (500 μM). Complete inhibition in DNA cleavage was observed in the presence of hydroxyl radical ($\cdot\text{OH}$) quenchers such as KI (500 μM), DMSO (6 μL), and catalase (4 units). The mechanistic results indicate the formation of $\cdot\text{OH}$ as the DNA cleaving agent. Addition of the DNA minor groove binder distamycin inhibited the cleavage activity of **1** but not of **2**, suggesting the minor and major groove binding propensity of the phen (**1**) and dppz (**2**) complexes, respectively. Further, the major groove binding affinity of complex **2** was evidenced from the inhibition of DNA cleavage in the presence of the DNA major groove binder methyl green.

To understand the role of the ferrocenyl unit in the DNA cleavage reactions, we explored the DNA cleavage activity of complex **1** and $[\text{Cu}(\text{L-met})(\text{phen})](\text{ClO}_4)$ under similar reaction conditions.²⁰ Significant enhancement in the DNA cleavage activity was observed for **1** in red light as compared to the activity of $[\text{Cu}(\text{L-met})(\text{phen})](\text{ClO}_4)$ (Figure S9 in the Supporting Information). While $[\text{Cu}(\text{L-met})(\text{phen})](\text{ClO}_4)$ is known to cleave DNA in red light via a singlet oxygen ($^1\text{O}_2$) pathway, the ferrocene-appended Cu(II) complexes form hydroxyl radicals as the cleavage active species.²⁰ This could be due to the presence of the ferrocene moiety that can form reactive $\{\text{Fe}(\text{III})-\text{Cu}(\text{I})\}$ species via a photoredox pathway, generating $\cdot\text{OH}$ radicals in a way similar to that reported by Sigman and co-workers for the $\{\text{Cu}^{\text{I}}(\text{phen})_2\}$ species, causing oxidative damage of the deoxyribose sugar moiety of DNA.^{21,22}

We investigated the interaction of the complexes with bovine serum albumin (BSA) protein.²³ Both complexes showed good BSA binding propensity, giving binding constant values (K_{BSA}) of 5.9×10^4 and $2.5 \times 10^5 \text{ M}^{-1}$ for **1** and **2**, respectively (Figure S10 in the Supporting Information). We also investigated the photoinduced BSA damage activity of the complexes (Figure 5). Complex **1** showed no apparent BSA cleavage activity in 365 nm UV-A light (100 W), while complex **2**, containing a dipyridophenazine ligand, exhibited efficient cleavage activity. A 50 μM solution of complex **2** showed complete damage of BSA upon photoexposure for 30 min. We observed complete fading of the BSA band intensity, possibly due to nonspecific binding of the complex to BSA.²⁴ The reactive species responsible for protein damage was found from mechanistic

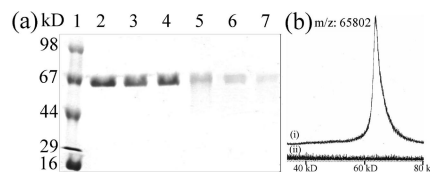


Figure 5. (a) 10% SDS-PAGE of BSA (4 μM) on photoexposure (t , min) to UV-A light of 365 nm (100 W) using the complexes **1** and **2** at 25 $^{\circ}\text{C}$: lane 1, standard molecular weight marker; lane 2, BSA control ($t = 30$ min); lane 3, BSA + **1** (50 μM ; $t = 30$ min); lane 4, BSA + **2** (50 μM , dark control); lane 5, BSA + **2** (25 μM ; $t = 30$ min); lane 6, BSA + **2** (50 μM ; $t = 15$ min); lane 7, BSA + **2** (50 μM ; $t = 30$ min). (b) MALDI-TOF MS traces of BSA on exposure to UV-A light of 365 nm for 30 min in the absence (i) and presence (ii) of the dppz complex **2**.

studies to be the $\cdot\text{OH}$ radical (Figure S11 in the Supporting Information).

In summary, we report here a new class of ferrocene-based amino acid reduced Schiff base ternary copper(II) complexes having planar phenanthroline bases showing efficient DNA binding propensity and significant DNA cleavage activity in red light within the PDT spectral window. We have observed a significant role of the ferrocene moiety in enhancing the DNA photocleavage activity in comparison to the mononuclear copper(II) complex. The presence of the Fc unit causes alteration of the mechanistic pathway from singlet oxygen to the hydroxyl radical pathway. The dppz complex shows UV-A light induced protein cleavage activity. The present work opens up a hitherto unexplored area in the PDT of organometallic complexes with suitable design for cellular applications in PDT targeting both primary and secondary tumors.

Acknowledgment. We thank the Department of Science and Technology (DST, Government of India) and the Council of Scientific and Industrial Research (CSIR), New Delhi, for financial support (Nos. SR/S5/MBD-02/2007 and 01-2081/06/EMR-II). We also thank the Alexander von Humboldt Foundation, Germany, for donation of an electroanalytical system. T.K.G. is grateful to the CSIR for a research fellowship. A.R.C. thanks the DST for a J. C. Bose National Fellowship.

Supporting Information Available: A CIF file giving crystallographic data for **1a** and figures, tables, and text giving ESI-MS (Figures S1 and S2), a cyclic voltammogram (Figure S3), electronic spectra (Figure S4), an ORTEP view and the unit cell packing diagram of **1** \cdot PF₆ (Figures S5 and S6), DNA binding plots (Figures S7 and S8), an agarose gel diagram (Figure S9), a BSA binding plot (Figure S10), a PAGE diagram (Figure S11), physicochemical data and crystallographic details (Tables S1–S3), and experimental details. This material is available free of charge via the Internet at <http://pubs.acs.org>.

OM900012B

(20) Patra, A. K.; Dhar, S.; Nethaji, M.; Chakravarty, A. R. *Chem. Commun.* **2003**, 1562–1563.

(21) Sigman, D. S. *Acc. Chem. Res.* **1986**, *19*, 180–186.

(22) Burrows, C. J.; Muller, J. G. *Chem. Rev.* **1998**, *98*, 1109–1152.

(23) Seetharamappa, J.; Kamat, B. P. *Chem. Pharm. Bull.* **2004**, *52*, 1053–1057.

(24) Tanimoto, S.; Matsumura, S.; Toshima, K. *Chem. Commun.* **2008**, 3678–3680.